Current Applied Science and Technology Vol. 22 No. 3 (May-June 2022)

Research article

TiO_2/SiO_2 Coated 310S Stainless Steel for Hydrogen Peroxide Generation via Photocatalytic Reaction

Tanongsak Sukkasem[1], Aroonsri Nuchitprasittichai[1], Pattanapong Janphuang[2] and Supunnee Junpirom[1]*

[1]*School of Chemical Engineering, Institute of Engineering, Suranaree University of Technology, Nakhon Ratchasima, Thailand*
[2]*Synchrotron Light Research Institute, Nakhon Ratchasima, Thailand*

Received: 2 February 2021, Revised: 18 June 2021, Accepted: 11 August 2021

DOI: 10.55003/cast.2022.03.22.001

Keywords

TiO_2/SiO_2;
photocatalysis;
hydrogen peroxide

Abstract

The photocatalytic reactor was designed by assembling the parts of a photocatalyst, an ultraviolet light source and an air distribution. This prototype reactor was used to generate H_2O_2 via photocatalytic reaction. TiO_2 and TiO_2/SiO_2 prepared from sol-gel method were coated on 310S stainless steel substrate using dip-coating technique. Rice husk ash was used as the source of SiO_2. The major phase of all the pure TiO_2 and SiO_2 particles was anatase and amorphous, respectively. The surface analysis showed the coated TiO_2 and TiO_2/SiO_2 with an average roughness of 365.391 and 1322.001 nm, respectively, compared with the average thickness of coated TiO_2 which was measured to be 2.7325 μm and for TiO_2/SiO_2, which was 4.7856 μm. The results also showed the coating of TiO_2/SiO_2 was highly porous at the surface compared with pure TiO_2. The TiO_2/SiO_2 show good photocatalytic reaction activity because SiO_2 doping on TiO_2 increased the adsorption of O_2 and H_2O molecules towards the photoactive center of TiO_2. Thus, the incorporation of SiO_2 onto the photocatalyst helped to increase photocatalytic activity. The generation of H_2O_2 increased with increasing ambient humidity up to 60% RH, but then decreased. This behavior was explained by the effect of water vapor adsorption on the SiO_2 surface. The air flowrate enhanced the generation of H_2O_2, higher air flow rate produced a higher amount of H_2O_2. H_2O_2 was generated at the highest concentration of 64 ppmv from the TiO_2/SiO_2 photocatalyst at ambient humidity of 60% RH and air flowrate 8.20 m/s.

*Corresponding author: Tel.: 0 4422 4245 Fax: 0 4422 4220
E-mail: supunnee@sut.ac.th

1. Introduction

The pandemic of COVID-19 is now the most challenging issue of mankind across the world. It was reported by World Health Organization (WHO), as of 8 June 2021, that the number of infections had reached 173 million confirmed cases [1]. The disinfection of pathogenic viruses, fungi, bacteria, molds, endospores, biofilms, organic and inorganic contaminants is now an interesting research area [2]. On the surfaces and in the atmosphere, these pathogens from various sources are widely distributed. There are various ways for disinfection such as physical and chemical methods [3]. Due to the mentioned problems, it is very interesting to design new sterilization processes that can kill or eliminate these microorganisms via an air purifier. However, the feasibility of such technology and processes must be carefully studied to ensure efficiency, safety and sustainability. Photocatalytic oxidation process is one way to destroy microorganisms and involves oxidizing organic contaminants [4].

One of the main members of the reactive oxygen species (ROS) group of molecules is hydrogen peroxide (H_2O_2), which is commonly considered to have antimicrobial properties, and tends to be an abundant molecule. Hydrogen peroxide is normally present in food and can be found in drinking water, rainwater and sea water [5-8]. Moreover, our lungs have enzymes that continuously convert oxygen and moisture in the lungs to hydrogen peroxide [9]. Hydrogen peroxide has been used for disinfection and microbial control in aqueous solutions. In today's efforts to use hydrogen peroxide gas, because the distribution of molecules in the gas phase is better than in liquid phase and it is particularly useful when the low concentration is available for operating. Recently, there has been a lot of effort to use hydrogen peroxide gas as the gas molecule is more able to diffuse through systems even at low concentration. Due to its rapid effectiveness, low temperature operation, surface compatibility and minimal toxicity issues, hydrogen peroxide gas-based processes have become common alternatives to other chemical and physical antimicrobial methods [10]. In addition, the Occupational Safety and Health Administration (OSHA) recommends that the safety level of vaporized hydrogen peroxide concentration lower that 1.0 ppm [11].

Most of the research concerning photocatalysis have been focused on oxidation processes, and the generation of hydrogen peroxide for use as an oxidizing agent [12]. Numerous research studies of photocatalytic processes have reported on the generation of hydrogen peroxide produced from hydrogen and oxygen from mixtures of water and alcohol, using ultraviolet light and a photocatalyst [13, 14]. In recent years, a wide range of photocatalyst, including TiO_2, ZnO, SnO_2, WO_3, CdS, ZrO_2, Sb_2O_4 and Fe_2O_3 have been investigated for their photocatalytic efficiency [15]. Titanium dioxide, in particular, have received a lot of research interest due to their catalytic activity. In order to increase the photocatalytic activity of TiO_2, the integration of TiO_2 with other agents, especially SiO_2, was found to induce reactant molecules to stay on the surface, a factor that when combined with sufficient ultraviolet light led to the reaction occurring more readily [16].

Several works have been studied on the use of TiO_2/SiO_2 photocatalyst in photocatalytic processes, such as the photocatalytic degradation of organophosphorus pesticides [17-26]. To synthesis the photocatalyst, the sol-gel technique was reported to be a simple and cost-effective process and this solution can be further used for coatings [27-30]. An important factor that influences photocatalytic reaction efficiency is the photocatalytic reactor's design because photocatalytic efficiency is highly dependent on light absorption. The immobilization of the catalyst onto a substrate is the basis of photocatalytic reactors for air reactions. Surface hydroxyl content, film thickness, and substrates all impact the gas-solid reaction that occurs on the catalyst thin film [31-33]. The flat plate reactor is the most often utilized gas phase reactor [34-36]. Thus, 310S stainless steel plates are of great interest. They can serve as catalyst support materials in photocatalytic reactors for air reactions. The stainless steel 310S is made from austenitic heat resistant alloy with

excellent oxidation resistance at 1093.33°C under mildly cyclic conditions and allow better air flow than quartz plates and other materials.

In this work, the dip-coating of 310S stainless steel substrates with TiO_2/SiO_2 prepared by the sol-gel method were developed to use as photocatalyst. The prepared photocatalyst was used as part of the assembly of a prototype device to generate hydrogen peroxide gas from ambient humidity air via photocatalytic reaction. Rice husk ash was used as the source of silicon dioxide. The physical and chemical characteristics of TiO_2 and TiO_2/SiO_2 catalysts on 310S stainless steel were investigated. The concentration of generated hydrogen peroxide was measured with variation of air relative humidity and air flowrate.

2. Materials and Methods

2.1 Preparation of TiO_2 and TiO_2/SiO_2 photocatalyst

2.1.1 Chemicals

Titanium (IV) butoxide reagent grade (97% (v/v) Sigma), ethanol absolute grade (99.9% (v/v)), sulfuric acid (98% (v/v)) and hydrochloric acid (37% (v/v) of ANaPURE) were purchased from New Zealand. Nitric acid (65% (v/v)), acetylacetone and hydrogen peroxide (30% (v/v)) were purchased from CARLO ERBA reagents, France. Rice husks were obtained from the local rice mill located in Nakhon Ratchasima, Thailand.

2.1.2 Preparation of amorphous SiO_2 powder

Amorphous SiO_2 powder was prepared as previously published [16]. First, a bulk 100g of rice husk, rich in silica, was rinsed in 1 l of sulfuric acid solution with concentration of 0.5 M at 80°C for 2 h, then rinsed again with water until pH equal to 7 was obtained. After rinsing, the rice husk was dried at 105°C for 24 h, then calcined in furnace with the heating rate set at 5°C/min, holding at 600°C, for 2 h. The obtained product was amorphous SiO_2.

2.1.3 Preparation of TiO_2 and TiO_2/SiO_2 photocatalyst solution via sol-gel method

TiO_2 and TiO_2/SiO_2 catalysts were prepared via the Sol-gel method. The preparation of TiO_2 photocatalyst solution was started by mixing the titanium (IV) n-butoxide 68 ml with ethanol absolute 210 ml, HNO_3 2.56 ml, DI water 5.5 ml and acetylacetone 10.4 ml. For the preparation of TiO_2/SiO_2 photocatalyst solution, the fixed ratio of 1:0.76% (w/w) of TiO_2:SiO_2 was used [16]. SiO_2 prepared from rice husk was added. Then the solution was stirred for 8 h at 200 rpm and at 80°C. After stirring, the solution was further left for 24 h to achieve the gel solution and it was a liquid and solid solution mixed.

2.2 Preparation of photocatalyst coated 310S stainless steel

2.2.1 Coating of the 310S stainless steel substrates

Each 310S stainless steel plate had a diameter of 130 mm with a thickness of 1 mm. Each plate was perforated with hole sizes of 1 mm across the plane surface. The first step was the surface treatment of the stainless steel to ensure maximum adhesion between the coating layer and the substrate.

During this process, all plates were immersed in molar 1:1 with sulfuric acid and hydrogen peroxide for 30 min. Each plate was then rinsed with DI water. Finally, the plates were dried at 100ºC.

The dip coating technique was selected for use in this work. Each plate was initially covered by tape on the smooth surface near the edge of the plate. Thus, after coating, the photocatalyst was attached on the surface zone of perforation. After coating, the plate was left to dry overnight at room temperature. Finally, the dried coated plates were calcined at temperature of 600°C for 2 h.

The sols were filled with powders prepared by firing gels of the same composition, with the maximum thickness for preparing thicker layers. Until a homogeneous mixture was obtained, these powders were introduced into the sols under stirring. This technique allows good quality thick layers to be prepared because the shrinkage during the drying stage was significantly reduced.

2.2.2 Characterization of catalysts

X-ray diffraction measurements (XRD) were carried out using a traditional Bragg-Brentano diffractometer with Ni-filtered Cu Kα radiation to identify the crystalline phases of the heat-treated powder samples. A field emission scanning electron microscope (FESEM) and energy dispersive X-ray spectroscope (EDS) were used to analyze the materials' morphologies. Measurements of roughness and thickness of TiO_2 and TiO_2/SiO_2 films were performed using a Brucker Contour GT profiler, which was used to measure thickness at each point in the field of view, a process that illustrated thickness variations.

2.3 Hydrogen peroxide generator

2.3.1 Photocatalytic reactor system and its operating method

A prototype of the photocatalytic reactor was assembled, as shown in Figure 1. The frame is an acrylic cylindrical vessel with legnth of 240 mm, inside dameter of 100 mm, and the thickness of 10 mm. The stainless steel plate which was coated with photocatalyst, was placed vertically inside the horizontal vessel. The UV lamp was inserted inside the vessel and fixed near the front of photocatalyst plate. A small fan with adjustable flow rate of air was attached in the front of the vessel. A device for measurement of the air flow rate was placed inside the vessel and put in after the fan. A probe to measure the generated hydrogen peroxide was inserted in the vessel and it was put after the photocatalyst plate. This probe was a model HPP272 supplied by Vaisala indigo 210, Finland. A smaller fan was also put at the end of the vessel to blow out the generated product gas to the surroundings. For the relative humidity variation, a control box, as shown in Figure 2 (a), was connected with the reactor vessel. The air humidifier was put inside this box and used for controlling the relative humidity. In Figure 2 (c), this box was connected with the reactor to simulate a surrounding volume to measure the distribution of generated hydrogen peroxide.

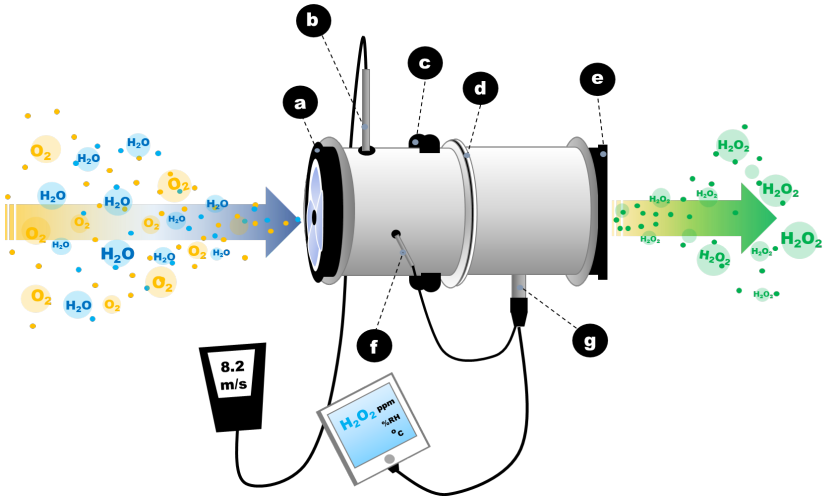

Figure 1. Schematic of photocatalytic reactor for hydrogen peroxide generation
(a) fan, (b) air flow meter, (c) UV light source, (d) 310S stainless steel plate, (e) ventilation fan, (g) hydrogen peroxide meter, and (f) ambient temperature humidity meter

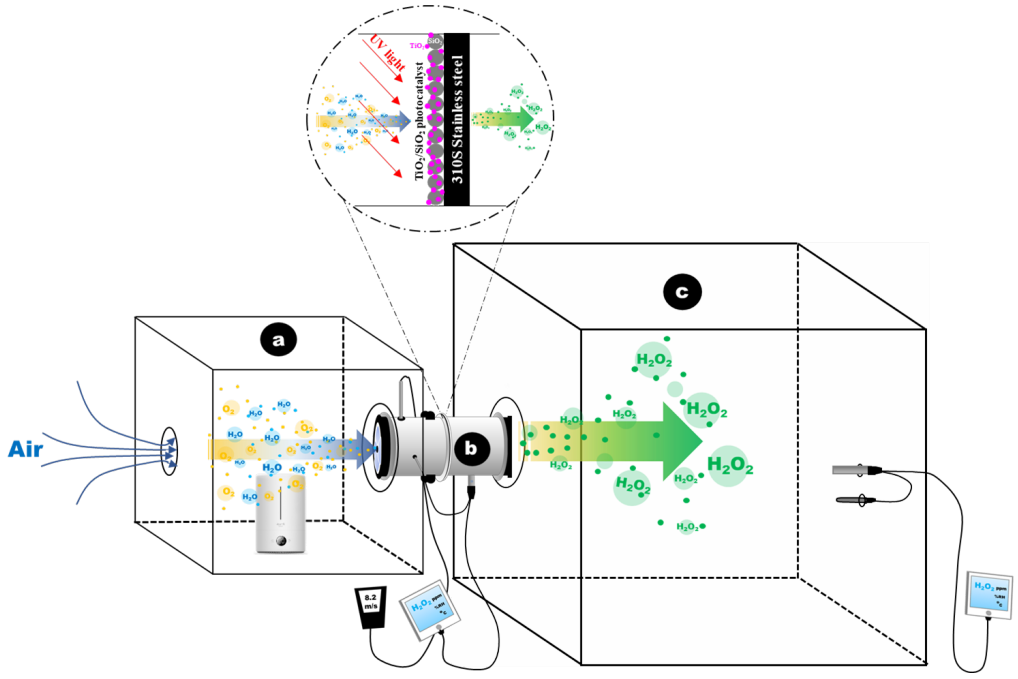

Figure 2. Schematic of (a) chamber for controlling humidity of air, (b) prototype photocatalytic reactor, and (c) chamber for measuring hydrogen peroxide distribution

3. Results and Discussion

3.1 Characterization of TiO_2 and TiO_2/SiO_2 photocatalyst

3.1.1 Analysis of photocatalysts synthesis

Figure 3 shows the FESEM micrographs of SiO_2, TiO_2 and TiO_2/SiO_2 powder. Apparently, SiO_2 had a rougher surface structure than that of TiO_2. The porous structure of SiO_2 was created by removing the existing organic molecules as volatile chemicals [37]. The resulting structure of SiO_2 after calcination at 600°C for 2 h created porous SiO_2 composite (Figure 3a). The TiO_2 crystal surface was quite smooth (Figure 3b). The synthesis of TiO_2/SiO_2 photocatalysts with the dispersion of SiO_2 on the surface increased the porosity of the structure (Figure 3c).

In Figure 4, after calcination at 600°C for 2 h, XRD patterns and crystalline phase content (anatase type TiO_2) were observed. Anatase (JCPDS card no. 84-1286) peaks were found at 2θ values of 25.4°, 37.0°, 38.0°, 38.8°, 48.0°, 54.0°, 55.2°, 62.9°, 68.9° and 70.5°. These corresponded to the (101), (103), (004), (112), (200), (105), (211), (118), (116), and (220) crystal planes. No diffraction peak of silica was observed in the XRD patterns, showing that silica in rice husk ash was still amorphous.

Figure 5 shows the FESEM/EDS images of SiO_2, TiO_2 and TiO_2/SiO_2 powder. The analyzed elements are O, Si, and Ti. In Figure 5a, the SiO_2 analysis showed the average weight and atomic percentage of Si and O were 42.69 and 57.31 wt.%, 29.81 and 70.19 ac.%, respectively. Figure 5b, the TiO_2 analysis indicted the average weight and atomic percentage of Ti and O were 75.77 and 24.23 wt.%, 51.10 and 48.90 ac.%, respectively. In Figure 5c, the TiO_2/SiO_2 analysis showed the average weight and atomic percentage of Ti, Si and O were 41.63, 19.98 and 38.39 wt.%, 21.87, 17.87 and 60.26 ac.%, respectively. These results indicated that TiO_2 particles were well dispersed with the SiO_2.

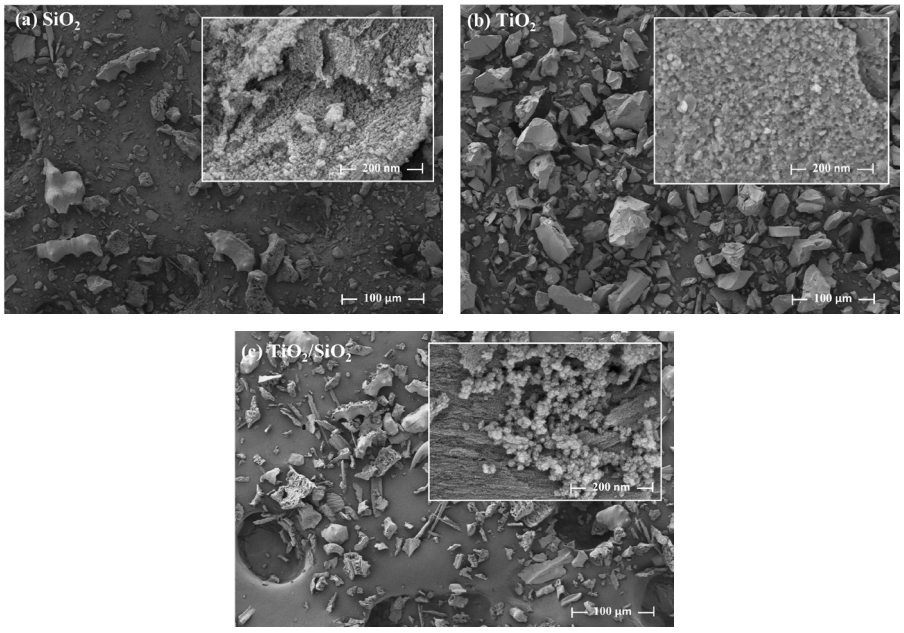

Figure 3. FESEM micrograph of samples (a) SiO_2, (b) TiO_2, and (c) TiO_2/SiO_2 powder

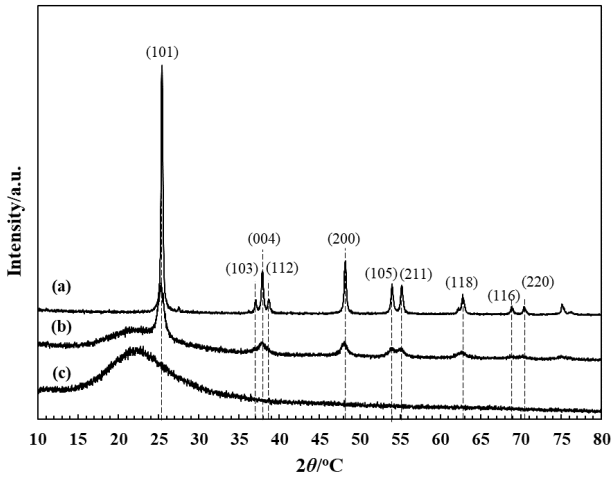

Figure 4. XRD patterns of photocatalysts (a) TiO_2, (b) TiO_2/SiO_2, and (c) SiO_2

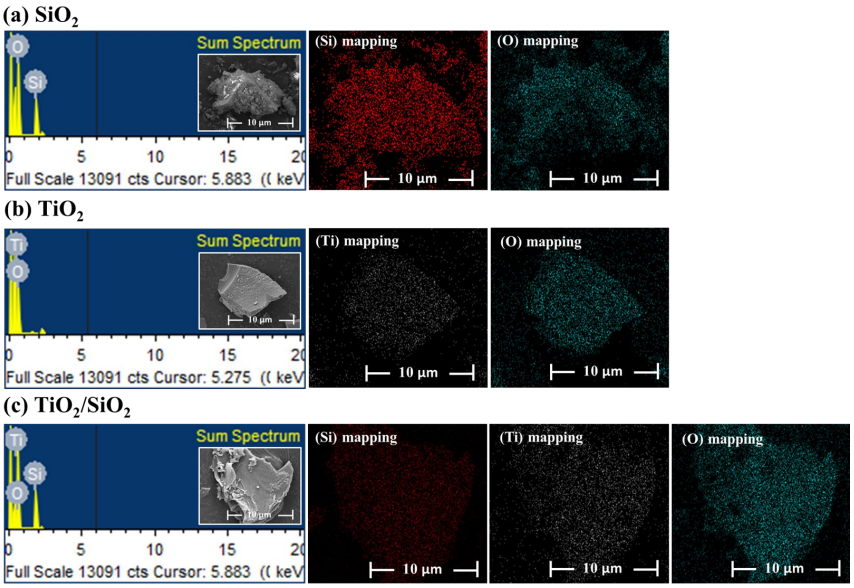

Figure 5. FESEM/EDS images of samples (a) SiO_2, (b) TiO_2, and (c) TiO_2/SiO_2 powder

3.1.2 Surface analysis and 301S stainless steel coated photocatalysts

The chemical composition of the uncoated 310S stainless steel used in this study (in wt.%) was provided by the supplier and consisted of Cr 24.8, Ni 19.1, C 0.069, Si 0.75, Mn 1.37, P 0.036, S <0.001, O 0.013, Cu 0.07, Al 0.07, Ti 0.010, N 0.062 and the balance Fe [38]. The uncoated surface was characterized and it was found that the surface was quite smooth, as show in Figure 6.

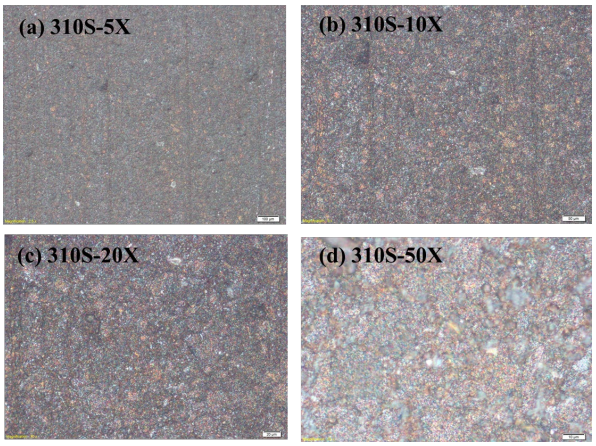

Figure 6. Microstructure of the uncoated 310S stainless steel

Studies on the surface roughness of uncoated and coated TiO_2 and TiO_2/SiO_2 photocatalyst on 310S stainless steel surface were done. During measurements, two-dimensional and three-dimensional parameters of surface roughness were also determined, and height (*Sa, Sku, Sp, Sq, Ssk, Sv, Sz*) was included. In fact, the topographic roughness of TiO_2/SiO_2 was the greatest, a finding reported in Table 1 that confirmed our qualitative findings. It was computed for both average roughness (*Sa*) (~1322 nm) and the root mean square roughness (*Sq*) (~1556 nm). Furthermore, the topographic pattern is comparable for maximum peak height (*Sp*), maximum pit height (*Sv*), and maximum height (*Sz*), indicating that topographic patterns in TiO_2/SiO_2 are significantly different from TiO_2 and uncoated photocatalysts. The asymmetry, or dissimilarity to a Gaussian distribution, is determined by the surface skewness (*Ssk*), which is related to the third momentum of the height distribution. Positive *Ssk*, such as turned surfaces, have relatively high spikes that protrude above a flatter average. Negatively *Ssk*, a feature of porous surfaces, contains relatively deep valleys inside a smoother plateau [39]. The surface kurtosis (*Sku*) value is a measurement of the roughness profile sharpness, above the mean plane, and the height distribution is skewed (*Sku*<3). The distribution of heights was normal (Parts that are sharp and parts that are indented coexist) (*Sku=3*), and height distribution was spiked (*Sku>3*). Figure 7 shows the surface roughness in 2D and 3D. The average roughness of the uncoated surface was 310.981 nm. The surface roughness of coated TiO_2 and TiO_2/SiO_2 were approximately 365.391 nm and 1322.001 nm, respectively. From these results, it indicates that coating with TiO_2/SiO_2 gave the surface higher thickness and surface roughness as well as porosity, as previously mentioned.

Figure 8 shows 2D and 3D analyses of the thickness of coated surface with different photocatalysts. The coated thickness of TiO_2 and TiO_2/SiO_2 were found to be 2.7325 μm and 4.7856 μm, respectively.

The microstructural characteristics of the coated 310S stainless steel with photocatalyst via the sol-gel using dip-coating technique were analyzed. The SEM images of the coated surface for TiO_2 and TiO_2/SiO_2 photocatalyst coating with different magnitudes are shown in Figure 9. As seen from Figure 9 (a)-(d), the TiO_2 coated surface possesses a regular crystal morphology and quite smooth surface. The average size of crystal is about 16.13 μm. The TiO_2/SiO_2 coated surface can be seen in Figure 9 (e)-(h), and this surface exhibits a porous surface structure. It was found that the average size of crystal was about 14.47 μm and the porous size was approximately 372.88 nm. However, due to the burning-out of organic compounds from rice husk, these vaporized molecules left the porous structure. Therefore, a network of pores was created in the silica surface.

Table 1. Value of the 2D and 3D surface roughness parameters

	2D and 3D						
310S Sample	***Sa*** **(nm)**	***Sku*** **–**	***Sp*** **(nm)**	***Sq*** **(nm)**	***Ssk*** **–**	***Sv*** **(nm)**	***Sz*** **(nm)**
Uncoated	310.981	10.426	1378.222	439.913	-1.978	-3415.035	4793.257
Coated TiO_2	365.391	4.915	2230.068	501.739	0.520	-2293.282	4523.350
Coated TiO_2/SiO_2	1322.001	2.093	3938.382	1556.645	0.192	-3479.549	7417.930

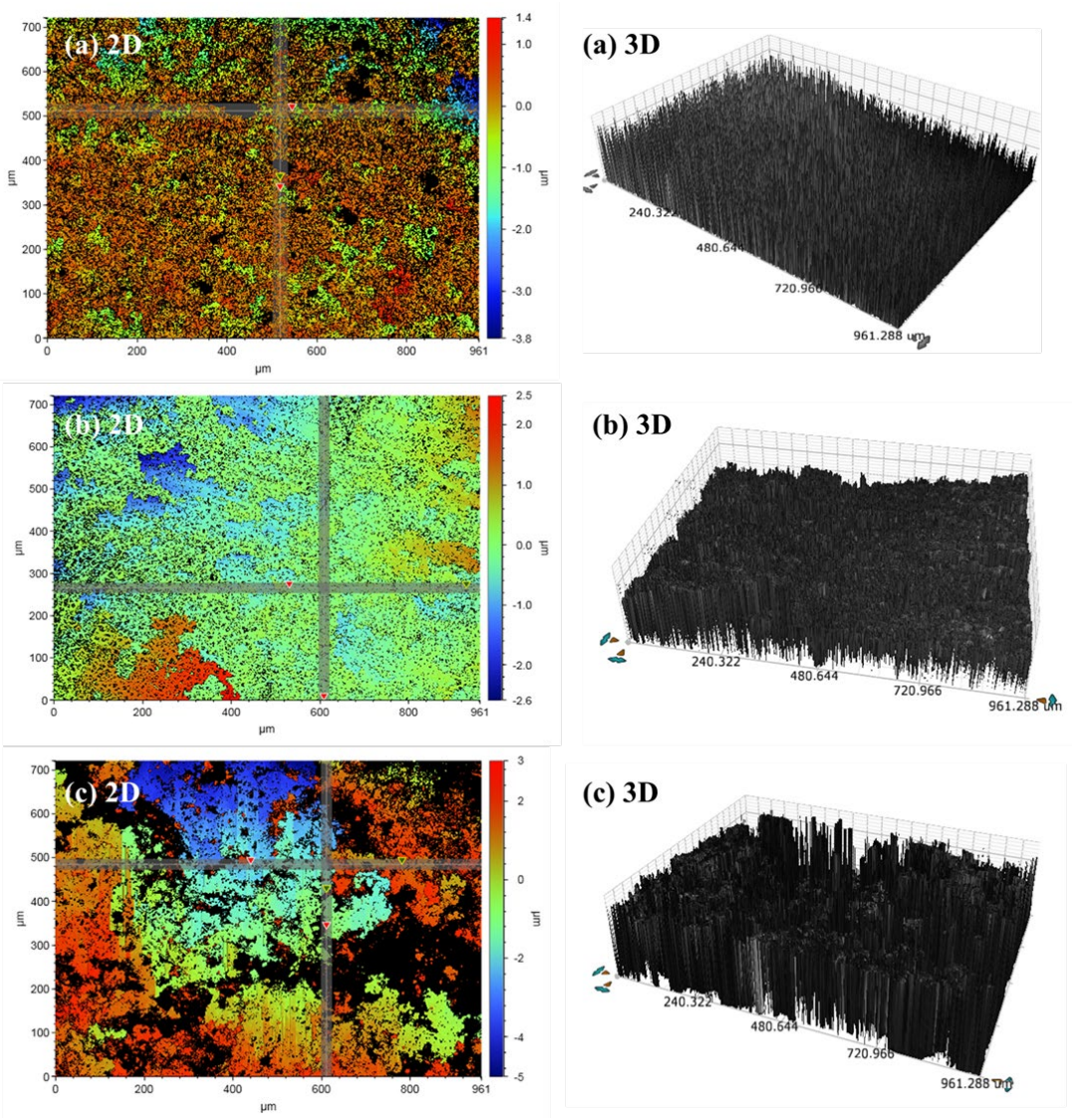

Figure 7. Surface roughness with 2D and 3D
(a) uncoated photocatalysts (b) coated TiO_2 (c) coated TiO_2/SiO_2

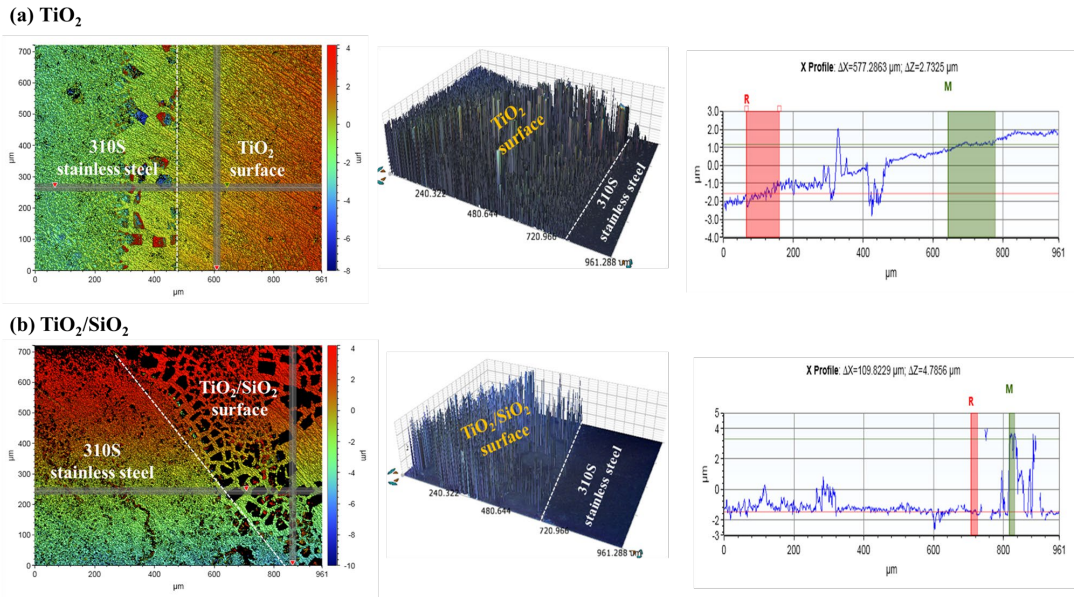

Figure 8. Show the thickness after coating TiO_2 and TiO_2/SiO_2 photocatalysts

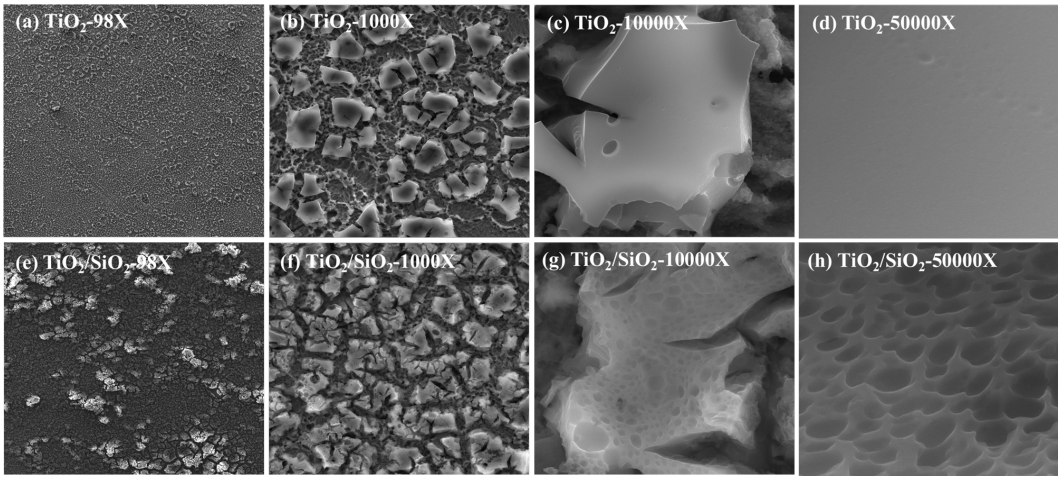

Figure 9. SEM micrograph of a TiO_2 and TiO_2/SiO_2 photocatalyst coated on 310S stainless steel

3.2 Photocatalytic reactor for hydrogen peroxide gas generation

3.2.1 Dry hydrogen peroxide generation with TiO_2 and TiO_2/SiO_2 photocatalyst

Figure 10 shows the time courses photocatalytic reactor operation and concentration of dry hydrogen peroxide generation with UV light, ambient humidity of air 60% RH, temperature 30°C and TiO_2/SiO_2 photocatalyst for photocatalytic reactor tests the same condition. Photocatalytic reactor testing for hydrogen peroxide synthesis was done to ensure that the reactor can synthesize in the same conditions. The test was performed three times.

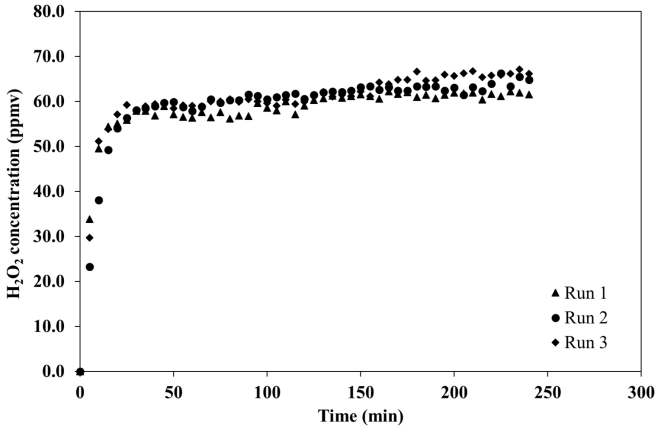

Figure 10. Time courses photocatalytic reactor operation and concentration of dry hydrogen peroxide generation with UV light, ambient humidity of air 60% RH, temperature 30°C, air velocity of 8.2 m/s, and TiO_2/SiO_2 photocatalyst for photocatalytic reactor tests

Figure 11 shows the time courses for the photocatalytic reactor operation and concentration of dry hydrogen peroxide generation with UV light, air flow rate 5.1 m/s, ambient humidity of air 60% RH and temperature 30°C of a comparison of TiO_2 and TiO_2/SiO_2 coated surfaces. The blank tests were run for without UV light and without photocatalyst, and as expected, no reaction occurred. However, a low concentration of dry hydrogen peroxide was detected due to its existence in the environment [5-9]. The TiO_2/SiO_2 photocatalyst appeared to give higher concentrations of hydrogen peroxide than the TiO_2 photocatalyst. Thus, the incorporation of SiO_2 into the photocatalyst helped increase photocatalytic activity. Due to the simultaneous functions of TiO_2 and SiO_2 as photocatalyst and adsorbent binary mixed oxide, TiO_2/SiO_2 proved to be a superior photocatalyst to TiO_2 alone. According to the mechanism shown in Figure 12, the addition of SiO_2 to the structure of TiO_2 significantly improved the specific surface area of TiO_2 based photocatalysts. Because of its high porosity, TiO_2/SiO_2 had a large surface area. Structures with high porosity have a large internal surface area per unit mass, which gives great accessibility and diffusivity, allowing molecules to pass through pores, resulting in increase in the adsorbed molecules breakdown on the catalyst's surface. The doping of SiO_2 on TiO_2 increased the adsorption of O_2 and H_2O molecules towards the photoactive center of TiO_2, and more molecules were broken down, resulting in a rapid degradation rate under UV light.

3.2.2 Relationship between ambient humidity and dry hydrogen peroxide generation with TiO_2/SiO_2 photocatalyst

Figure 13 shows the time course photocatalytic reactor operation and concentration of dry hydrogen peroxide generation with UV light, air flow rate 5.1 m/s, temperature 30°C and TiO_2/SiO_2 photocatalyst for different relative humidity. The humidity fed into photocatalytic reactor has an effect on the photocatalytic reaction for hydrogen peroxide generation. It was found that increasing the relative humidity up to 60% increased the concentration of generated hydrogen peroxide. However, at the 70% RH the concentration of generated hydrogen peroxide was lower than that at 60% RH. The results may have been due to the effect of water adsorption by the SiO_2 porous structure as represented in Figure 14. In Figure 14 (a)-(b), at the low relative humidity, molecules of water were mostly trapped or adsorbed inside the pore of SiO_2. Thus, there was a small portion

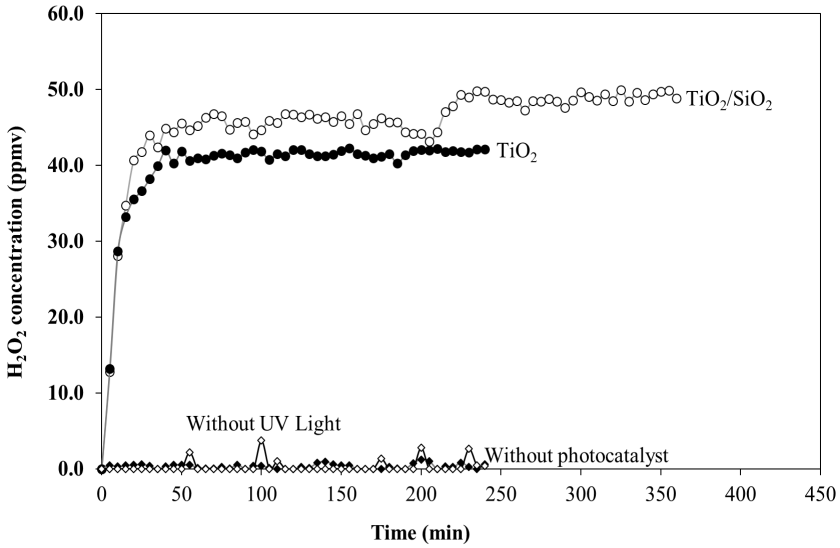

Figure 11. Time courses photocatalytic reactor operation and concentration of dry hydrogen peroxide generation with UV light, air flow rate 5.1 m/s, ambient humidity of air 60% RH, and temperature 30°C for TiO_2 and TiO_2/SiO_2

of the free water molecules left in the bulk stream to react by photocatalytic mechanism and become hydrogen peroxide. When the relative humidity reached 60% (Figure 14 (c)), the SiO_2's pores were full with water molecules. The portion of free water molecules in bulk phase was quite large, and these molecules were reacted to generate hydrogen peroxide. However, when the relative humidity was at 70% (Figure 14 (d)), the portion of free water molecules in bulk phase was excessive, leading to some water molecules covering or accumulating on the active sites. These active sites then became inactive, and the concentration of generated hydrogen peroxide decreased.

3.2.3 Relationship between velocity of ambient humidity and dry hydrogen peroxide generation with TiO_2/SiO_2 photocatalyst

The time course for photocatalytic reactor operation and concentration of dry hydrogen peroxide generation for different air flowrate with UV light, ambient humidity of air 60% RH, temperature 30°C and TiO_2/SiO_2 photocatalyst is shown in Figure 15. It was found that increasing in the air flowrate increased the concentration of generated hydrogen peroxide. This trend may have been due to the higher flowrate giving a higher feed amount of water molecules into the system. Thus, a higher number of water molecules was photocatalyzed to hydrogen peroxide. The high flowrate also reduced film resistance at the active sites. From this reason, all active sites demonstrated good photocatalytic activity.

A comparison of this research with other studies regarding the photocatalytic production of hydrogen peroxide with TiO_2 based photocatalysts is shown in Table 2. In this study, hydrogen peroxide in gaseous form was synthesized at concentrations up to 64 ppmv (1.88 mM) after 1 h.

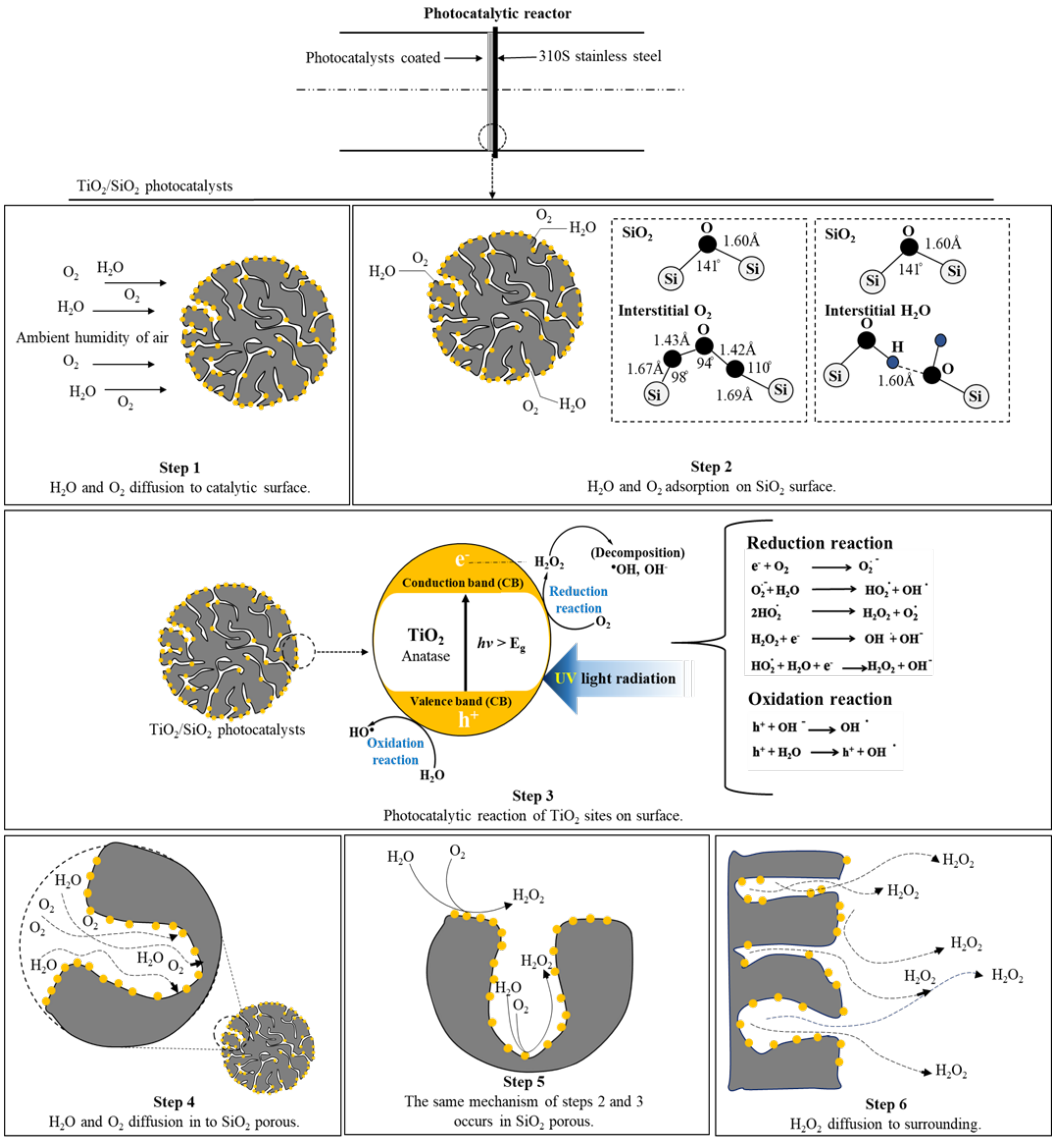

Figure 12. Mechanisms of photocatalytic reaction for hydrogen peroxide generation

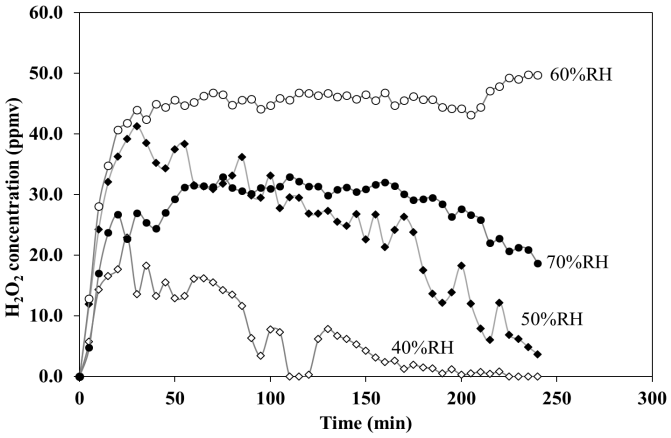

Figure 13. Time course photocatalytic reactor operation and concentration of dry hydrogen peroxide generation with UV light, air flow rate 5.1 m/s, temperature 30°C and TiO_2/SiO_2 photocatalyst for different relative humidities

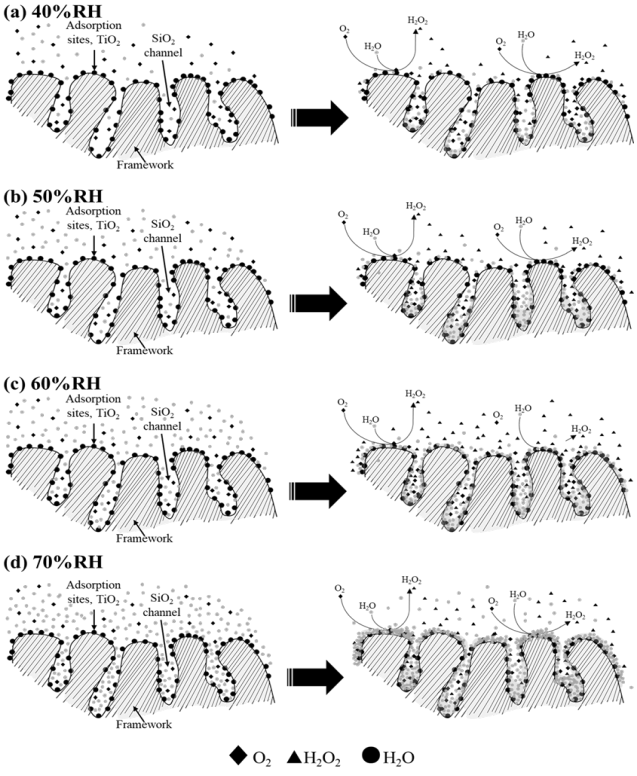

Figure 14. Schematic representation of the water adsorption in SiO_2's porosity and portion of free water molecules in bulk phase

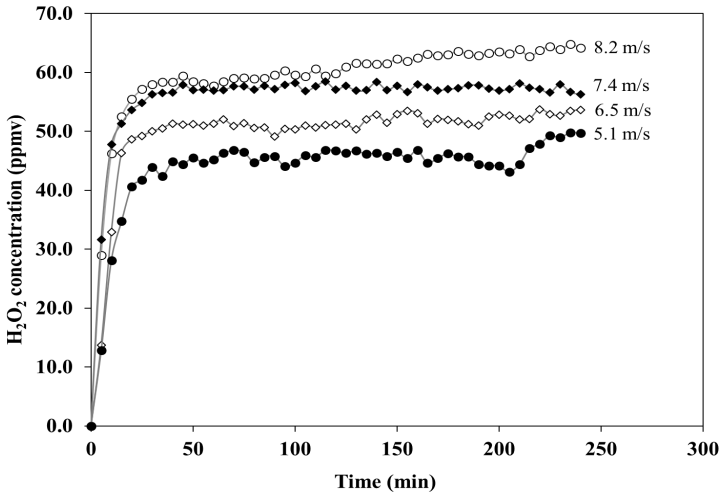

Figure 15. Time courses photocatalytic reactor operation and concentration of dry hydrogen peroxide generation with UV light, ambient humidity of air 60% RH, temperature 30°C and TiO_2/SiO_2 photocatalyst

Table 2. Summary of the photocatalytic production of H_2O_2 with TiO_2 based photocatalysts

Material	Sacrificial reagent	Irradiation conditions	H_2O_2 yield (1h)	Reference
TiO_2/SiO_2 (in this work)	Ambient humidity	UV	1.88 mM	-
Au/TiO_2	HCOOH	λ>420 nm	0.64-0.70 mM	[40]
TiO_2/rGO/carbon dots	2-propanol	AM 1.5	ca. 0.35 mM	[41]
TiO_2/WO_3/rGO	2-propanol	AM 1.5	ca. 0.27 mM	[42]
SN-GQD/TiO_2	2-propanol	λ>420 nm	0.451 mM	[43]
Co@TiO_2	CH_3OH	λ=400 nm	1.7 mM	[44]
SNG/TiO_2	2-propanol	λ≥300 nm	0.373 mM	[45]
Pt/TiO_2	-	Full spectrum	5.096 mM	[46]

4. Conclusions

TiO_2 and TiO_2/SiO_2 coatings were prepared by the sol-gel method and dip-coating technique on 310S stainless steel substrates. It was verified by SEM that the coating was highly porous on surface TiO_2/SiO_2 photocatalyst. The prototype photocatalytic reactor was designed by assembling the parts of photocatalyst, ultraviolet light source and air distribution system. The TiO_2/SiO_2 photocatalyst irradiated with UV light generated a high concentration of H_2O_2 from water vapor. The generation of dry hydrogen peroxide increased with increasing ambient humidity up to 60% RH, but then a decreasing trend was observed. This behavior was explained by the effect of water vapor adsorption on the SiO_2 surface. Air flowrate enhanced the generation of dry hydrogen peroxide, and higher air flow rate produced higher amounts of dry hydrogen peroxide. From all the tests in this investigation,

the prototype of photocatalytic reactor was able to generate a high concentration of dry hydrogen peroxide at 64 ppmv with ambient humidity at 60% RH, and air flowrate of 8.2 m⁄s.

5. Acknowledgements

This work was financially supported by the Technopolis, Suranaree University of Technology. The authors also gratefully acknowledge the support of the Synchrotron Light Research Institute (SLRI) and the Center of Excellence in Biomechanics Medicine.

References

[1] World Health Organization (WHO), 2021. *WHO Coronavirus Disease (COVID-19) Dashboard*. [online] Available at: http://www.worldometers. info/coronavirus/#countries.
[2] Smith, H., 1977. Microbial surfaces in relation to pathogenicity. *Bacteriological Reviews,* 41(2), 475-500.
[3] McKeen, L., 2012. *The Effect of Sterilization on Plastics and Elastomers*. 4th ed. New York: William Andrew.
[4] Thiruvenkatachari, R., Vigneswaran, S. and Moon, I.S., 2008. A review on UV/ TiO_2 photocatalytic oxidation process. *Korean Journal of Chemical Engineering,* 25(1), 64-72.
[5] Willey, J.D., Paerl, H.W. and Go, M., 1999. Impact of rainwater hydrogen peroxide on chlorophyll a content of surface gulf stream seawater off North Carolina, USA. *Marine Ecology Progress Series,* 178, 145-150.
[6] Price, D., Worsfold, P.J., Mantoura, R. and Fauzi, C., 1992. Hydrogen peroxide in the marine environment: cycling and methods of analysis. *Trends in Analytical Chemistry,* 11(10), 379-384.
[7] Szymczak, R. and Waite, T.D., 1991. Photochemical activity in waters of the Great Barrier Reef. *Estuarine, Coastal and Shelf Science,* 33(6), 605-622.
[8] Weller, R. and Schrems, O., 1993. H_2O_2 in the marine troposphere and seawater of the Atlantic Ocean (48ºN-63ºS). *Geophysical Research Letters,* 20(2), 125-128.
[9] Halliwell, B., Clement, M.V. and Long, L.H., 2000. Hydrogen peroxide in the human body. *FEBS Letters,* 486(1), 10-13.
[10] McDonnell, G., 2014. The use of hydrogen peroxide for disinfection and sterilization application. *PATAI'S Chemistry of Functional Groups,* 2014, 1-34.
[11] United States Department of Labor, 2019. *Occupational Safety and Health Administration (OSHA)*. [online] Available at: http://www.osha.gov/dts/sltc/methods/inorganic/id006/ hydrogen_peroxide. html.
[12] Finnegan, M., Linley, E., Denyer, S.P., McDonnell, G., Simons, C. and Maillard, J.-Y., 2010. Mode of action of hydrogen peroxide and other oxidizing agents: differences between liquid and gas form. *The Journal of Antimicrobial Chemotherapy,* 65(10), 2108-2115.
[13] Shiraishi, F., 2003. Formation of hydrogen peroxide in photocatalytic reaction. *The Journal of Physical Chemistry A,* 107(50), 11072-11081.
[14] Jack, H., 2003. The direct formation of H_2O_2 from H_2 and O_2 over palladium Catalyst. *Journal of Catalysis,* 216(1-2), 455-460.
[15] James, D.L. and Douglas, J.B., 2019. *Purified Hydrogen Peroxide Gas Generation Method and Devices*, U.S. Pat. 10,232,076.
[16] Klondon, R., 2013. *Removal of Air Pollutants by Photocatalytic Process Using TiO_2/SiO_2 Coated Dan Kwian Pottery*. M.Eng. Suranaree University of Technology, Thailand.

[17] Shifu, C. and Gengyu, C., 2005. Photocatalytic degradation of organophoshorus pesticides using floating photocatalyst TiO_2·SiO_2/beads by sunlight. *Solar Energy,* 79, 1-9.
[18] Yamashita, H., Kawasaki, S., Ichihashi, Y., Harada, M., Anpo, M., Stewart, M., Fox, M.A., Louis, C. and Che, M., 1998. Characterization of titanium-silicon binary oxide catalysts prepared by the sol-gel method and their photocatalytic reactivity for the liquid-phase oxidation of 1-octanol. *The Journal of Physical Chemistry B,* 102, 5870-5875.
[19] Tanaka, T., Teramura, K., Yamamoto, T., Takenaka, S., Yoshida, S. and Funabiki, T., 2002. TiO_2/SiO_2 photocatalysts at low levels of loading: preparation, structure and photocatalysis. *Journal of Photochemistry and Photobiology A: Chemistry,* 148(1-3), 277-281.
[20] Malinowska, B., Walendziewski, J., Robert, D., Weber, J.V. and Stolarski, M., 2003. The study of photocatalytic activities of titania and titania-silica aerogels. *Applied Catalysis B: Environmental,* 46, 441-451.
[21] Jung, K.Y. and Park, S.B., 2004. Photoactivity of SiO_2/TiO_2 and ZrO_2/TiO_2 mixed oxides prepared by sol-gel method. *Material Letters,* 58, 2897-2900.
[22] Chen, Y., Wang, K. and Lou, L., 2004. Photodegradation of dye pollutants on silica gel supported TiO_2 particles under visible light irradiation. *Journal of Photochemistry and Photobiology A: Chemistry,* 163, 281-287.
[23] Jin, M., Zhang, X., Emeline, A.V., Liu, Z., Tryk, D.A., Murakami, T. and Fujishima, A., 2006. Fibrous TiO_2-SiO_2 nanocomposite photocatalyst. *Chemical Communications,* 2006(43), 4483-4485.
[24] Zhang, M., An, T., Fu, J., Sheng, G., Wang, X., Hu, X. and Ding, X., 2006. Photocatalytic degradation of mixed gaseous carbonyl compounds at low level on adsorptive TiO_2/SiO_2 photocatalyst using a fluidized bed reactor. *Chemosphere,* 64(3), 423-431.
[25] Maldotti, A., Molinari, A., Amadelli, R., Carbonell, E. and Garcia, H., 2008. Photocatalytic activity of MCM-organized TiO_2 materials in the oxygenation of cyclohexane with molecular oxygen. *Photochemical and Photobiological Science,* 7, 819-825.
[26] Hu, C., Tang, Y., Yu, J.C. and Wong, P.K., 2003. Photocatalytic degradation of cationic blue X-GRL adsorbed on TiO_2/SiO_2 photocatalyst. *Applied Catalysis B: Environmental,* 40, 131-140.
[27] Shanaghi, A., Aghdam, A.S.R., Shahrabi, T. and Aliofkhazraee, M., 2009. Corrosion protection of mild steel by applying TiO_2 nanoparticle coating via sol-gel method. *Protection of Metals and Physical Chemistry of Surfaces,* 45(3), 305-311.
[28] Shanaghi, A., Rouhaghdam, A.S., Shahrabi, T. and Aliofkhazraei, M., 2008. Study of TiO_2 nanoparticle coatings by the sol-gel method for corrosion protection. *Material Science,* 44(2), 71-81.
[29] Shen, G.X., Chen, Y.C. and Lin, C.J., 2005. Corrosion protection of 316 L stainless steel by a TiO_2 nanoparticle coating prepared by sol-gel method. *Thin Solid Films,* 489, 130-136.
[30] Mendoza, E. and García, C., 2007. Sol-gel coatings deposited on stainless steels alloys review. *Dyna,* 74(153), 101-110.
[31] Yu, J.G., Zhao, X.J., Du, J.C. and Chen, W.M., 2000. Preparation, Microstructure and photocatalytic activity of the porous TiO_2 anatase coating by sol-gel processing. *Journal of Sol-Gel Science and Technology,* 17, 163-171.
[32] Yu, J.G. and Zhao, X.J., 2000. Effect of substrates on the photocatalytic activity of nanometer TiO_2 thin films. *Material Research Bulletin,* 35, 1293-1301.
[33] Yu, J.G., 2002. Photocatalytic activity and characterization of the sol-gel derived Pb-doped TiO_2 thin films. *Journal of Sol-Gel Science and Technology,* 24, 39-48.
[34] Obee, T.N. and Hay, S.O., 1997. Effects of moisture and temperature on the photooxidation of ethylene on titania. *Environmental Science and Technology,* 31, 2034-2038.

[35] Puddu, V., Choi, H., Dionysiou, D.D. and Puma, G.L., 2010. TiO_2 photocatalyst for indoor air remediation: Influence of crystallinity, crystal phase, and UV radiation intensity on trichloroethylene degradation. *Applied Catalysis B: Environment,* 94, 211-218.

[36] Salvadó-Estivill, I., Brucato, A. and Puma, G.L., 2007. Two-dimensional modeling of a flatplate photocatalytic reactor for oxidation of indoor air pollutants. *Industrial and Engineering Chemistry Research,* 46(23), 7489-7496.

[37] Tang, M.M. and Bacon, R., 1964. Carbonization of cellulose fibers. Part I: Low temperature pyrolysis. *Carbon,* 2(3), 211-220.

[38] Amirkhiz, B.S., Xu, S. and Scott, C., 2019. Microstructural assessment of 310S stainless steel during creep at 800°C. *Materialia,* 6, 100330, https://doi.org/10.1016/j.mtla.2019.100330.

[39] Vilas, A.M., Bruque J.M. and Gonzalez-Martın, M.L., 2007. Sensitivity of surface roughness parameters to changes in the density of scanning points in multi-scale AFM studies. Application to a biomaterial surface. *Ultramicroscopy,* 107(8), 617-625.

[40] Kofuji, Y., Isobe, Y., Shiraishi, Y., Sakamoto, H., Ichikawa, S., Tanaka, S. and Hirai, T., 2018. Hydrogen peroxide production on a carbon nitride-boron nitride-reduced graphene oxide hybrid photocatalyst under visible light. *ChemCatChem*, 10(9), 2070-2077.

[41] Zeng, X., Wang, Z., Meng, N., McCarthy, D.T., Deletic, A., Pan, J.-H. and Zhang, X., 2017. Highly dispersed TiO_2 nanocrystals and carbon dots on reduced graphene oxide: Ternary nanocomposites for accelerated photocatalytic water disinfection. *Applied Catalysis B: Environmental,* 202, 33-41.

[42] Zeng, X., Wang, Z., Wang, G., Gengenbach, T.R., McCarthy, D.T., Deletic, A., Yu, J. and Zhang, X., 2017. Highly dispersed TiO_2 nanocrystals and WO_3 nanorods on reduced graphene oxide: Z-scheme photocatalysis system for accelerated photocatalytic water disinfection. *Applied Catalysis B: Environmental,* 218, 163-173.

[43] Zheng, L., Su, H., Zhang, J., Walekar, L.S., Molamahmood, H.V., Zhou, B., Long, M. and Hu, Y.H., 2018. Highly selective photocatalytic production of H_2O_2 on sulfur and nitrogen co-doped graphene quantum dots tuned TiO_2. *Applied Catalysis B: Environmental,* 239, 475-484.

[44] Baran, T., Wojtyła, S., Minguzzi, A., Rondinini, S. and Vertova, A., 2019. Achieving efficient H_2O_2 production by a visible-light absorbing, highly stable photosensitized TiO_2. *Applied Catalysis B: Environmental,* 244, 303-312.

[45] Zheng, L., Zhang, J., Hu, Y.H. and Long, M., 2019. Enhanced photocatalytic production of H_2O_2 by Nafion coatings on S,N-codoped graphene-quantum-dots-modified TiO_2. *The Journal of Physical Chemistry C,* 123(22), 13693-13701.

[46] Wang, L., Cao, S., Guo, K., Wu, Z., Ma, Z. and Piao, L., 2019. Simultaneous hydrogen and peroxide production by photocatalytic water splitting. *Chinese Journal of Catalysis*, 40, 470-475.